Optical Materials 143 (2023) 114148

Contents lists available at ScienceDirect

Optical Materials

journal homepage: www.elsevier.com/locate/optmat

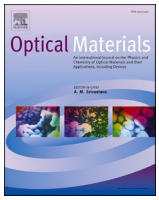

Research Article

Development of a new CoS-Supported $ZnAl_2O_4$ catalyst for the visible photodegradation of a basic textile dye from water

Youssef Fahoul [a], Karim Tanji [a,*], Oscar Manuel González Díaz [b], Raúl Quesada-Cabrera [b,c], Yassine Naciri [d], Imane El Mrabet [e], Abdelali El Gaidoumi [f], José Miguel Doña Rodríguez [b], Abdelhak Kherbeche [a]

[a] Laboratory of Materials, Process, Catalysis and Environment (LMPCE), Higher School of Technology, Sidi Mohamed Ben Abdellah University, B.P. 2427, Fez, Morocco
[b] Fotocatálisis y Espectroscopía para Aplicaciones Medioambientales (FEAM), Department of Chemistry, University Institute of Environmental Studies and Natural Resources (i-UNAT), Edificio Central del Parque Científico Tecnológico, Universidad de Las Palmas de Gran Canaria, Campus Universitario de Tafira, Las Palmas, 35017, Spain
[c] Department of Chemistry, Christopher Ingold Laboratories, University College London, 20 Gordon St., London, WC1H 0AJ, UK
[d] Laboratory of Materials and Environment, Faculty of Sciences, Ibnou Zohr University, Agadir, Morocco
[e] Department of Physics-Chemistry, Polydisciplinary Faculty of Ouarzazate, University of Ibnou Zohr, Ouarzazate, Morocco
[f] Laboratory of Biotechnology, Bioresources and Bioinformatics (3Bio), Higher School of Technology of Khenifra, Sultan Moulay Slimane University, Beni Mellal, Morocco

ARTICLE INFO

Keywords:
Basic textile dyes
Solar photocatalysis
Visible light illumination
Spinel structure
Supported materials

ABSTRACT

The material is proven competitive for the solar treatment of wastewater from the textile industry -an essential source of water pollution worldwide. The system was prepared following a two-step hydrothermal method, showing photon absorption properties across the solar spectrum's UV and visible light regions. The main responsible species driving the photocatalytic process are proposed based on degradation experiments using appropriate scavengers. Further studies include consideration of operational parameters and cycling experiments to evaluate the stability of the catalyst. The results showed complete degradation (100%) based on dye bleaching and >90% mineralization of the dye based on total organic carbon analysis using dye concentrations of 20 ppm and catalyst loading of 1 g/l. Our findings point to sulfide-supported spinel materials as promising candidates for advanced solar oxidation technologies for wastewater treatment.

1. Introduction

The textile industry is among the most polluting sources of water worldwide. A recent report [1] analysing the impact of measures to detox the clothing industry, highlighted the significant progress to cut down hazardous chemicals within the supply chains of fashion companies. Nevertheless, these changes represent only 15% of the global textile industry and untreated wastewater from textile processes is often discharged directly into rivers and streams. This situation is worsening with population growth and urbanisation, particularly with growing industries in areas away from a sewerage network and in remote locations, which is the case in many regions across North Africa and South-East Asia, for instance. Conveniently, these locations have abundant solar irradiation and thus they are ideal for the implementation of effective advanced oxidation processes (AOPs) based on photocatalytic mechanisms.

The principle of photocatalysis has been widely applied in the photodegradation of dyes, particularly using standard photocatalysts such as TiO_2 [2] and ZnO [3]. Other systems, such as TiO_2–SiO_2–Ag [4], Bi_2O_3–ZnO [5], Cu–ZnO [6] and Ag–TiO_2 [7], among others, have been designed to overcome some of the main issues with standard photocatalysts [8]. Spinel structures have attracted an interest in this area due to their catalytic efficiency, high surface area, stability and non-toxicity [9,10]. Conveniently, these materials show magnetic properties that can ease their separation from effluents after treatment.

Zinc aluminate spinel ($ZnAl_2O_4$) (Fig. 2S) is typified by its high chemical and thermal stability, mechanical resistance, good redox properties and low surface acidity, which promotes its use in a wide range of applications including the photodegradation of organic pollutants [11–14]. Unfortunately, $ZnAl_2O_4$ is a wide bandgap

* Corresponding author.
E-mail address: karim.tanji@usmba.ac.ma (K. Tanji).

https://doi.org/10.1016/j.optmat.2023.114148
Received 6 April 2023; Received in revised form 4 July 2023; Accepted 16 July 2023
Available online 25 July 2023

semiconductor (E_{bg}≈4 eV) and can only harvest high-energy photons (λ < 310 nm), which hinders its photocatalytic use under sunlight conditions. In order to enhance its photon absorption, spinel structures have been supported by narrow bandgap materials such as metal sulphides. Examples of these systems, such as CdS/$ZnFe_2O_4$ [15], have been successfully applied to photocatalytic processes.

In the present work, a cobalt sulphide (CoS)-supported $ZnAl_2O_4$ system was synthesised and evaluated during the degradation of a basic dye model, blue basic 41 (or BB41), under UV and visible light irradiation conditions. Basic dyes are used intensively in the textile industry due to their brightness and intense colour even at low concentrations. The band structure of CoS (Fig. 2S) is positioned within the bandgap of $ZnAl_2O_4$ thus favouring the transfer of photogenerated charges (h^+,e^-). In addition, CoS is a narrow bandgap semiconductor (E_{bg} = 1.6 eV) and thus it can harvest low energy photons (λ < 775 nm) across the entire visible range of the solar spectrum.

2. Materials and methods

2.1. Synthesis of CoS-supported $ZnAl_2O_4$ catalyst

All chemical precursors were purchased from *Sigma-Aldrich* and used without extra purification. The CoS-supported $ZnAl_2O_4$ catalyst (henceforth CoS–$ZnAl_2O_4$) was synthesised following a two-step method. The spinel structure was first prepared by a *sol-gel* method, the appropriate amounts of aluminium nitrate ($Al(NO_3)_3.9H_2O$) (7.5 g) and zinc nitrate ($Zn(NO_3)_2.6H_2O$) (2.97 g) were dissolved in deionized water and magnetically stirred for 30 min. Then, ammonia (NH_3 25%) was added to this solution under continuous stirring until complete precipitation at pH 8.5. The obtained mixture was filtered to separate the gel formed, washed with deionized water and dried at 100 °C for 24 h. Finally, the obtained solid was crushed and calcined at 750 °C (ramp 10 °C/min) for 3 h.

The as-prepared $ZnAl_2O_4$ was used as a substrate in the hydrothermal synthesis of CoS–$ZnAl_2O_4$, from a mixture of 0.84 g cobalt (II) chloride ($CoCl_26H_2O$) and 0.27 g thiourea ($SC(NH_2)_2$) in 90 mL ethylene glycol ($(CH_2OH)_2$). After the addition of 0.75 g of $ZnAl_2O_4$ powder, the dispersion was kept under stirring conditions for 30 min, followed by further sonication for 30 min. The mixture was poured into a Teflon-lined autoclave and annealed to 180 °C for 20 h. The autoclave was slowly cooled at room temperature and the obtained mixture was filtered and repeatedly washed with alcohol and deionized water. The final product was dried at 90 °C for 8 h.

Pristine cobalt sulfide (CoS) was synthesised following the same procedure but without the addition of $ZnAl_2O_4$ powder. This material was used as reference, as well as pristine $ZnAl_2O_4$. Commercial *P25* TiO_2 (*Aeroxide*) was used as a standard in these experiments.

2.2. Material characterisation

Structural characterisation was carried out using a Bruker D8 ADVANCE diffractometer under Cu $K\alpha_1$ radiation at 40 kV, 40 mA and 1.6 kW. VESTA structural analysis software was used to visualise the cubic and octahedral structures of $ZnAl_2O_4$ and CoS, respectively. The database of the Joint Committee on Powder Diffraction Standards (JCPDS) was used to identify the different phases. Cell parameters were obtained after refinement of X-ray diffraction patterns using the Fullprof software. Rough crystallite size of the as-prepared samples were estimated using the Scherrer equation ($D = K\lambda/(\beta\cos\theta)$) using the main characteristic peak and the most intense. X-ray photoelectron spectroscopy (XPS) was carried out on a Thermo Scientific K-alpha photoelectron spectrometer using monochromatic $Al_{k\alpha}$ radiation and a dual beam charge compensation system. Survey scans were measured in the range of 1–1200 eV. High resolution scans were recorded for the principal peaks of zinc (Zn 2p), aluminium (Al 2p), cobalt (Co 2p), sulphur (S 2p) and carbon (C 1s) at a pass energy of 50 eV. All peaks were calibrated to adventitious carbon (285.0 eV). A PerkinElmer Spectrum Two FT-IR Spectrometer was used to perform the Fourier transform infrared spectra (FTIR) analysis in the range of 450–4000 cm^{-1}. Morphological studies were carried out using a Jeol-IT500 HR Microscope under an acceleration voltage from 0.5 to 30 KV. The EDAX analysis was done using Hitachi TM3030 Scanning Electron Microscope (SEM) and EDAX Bruker micro analytic probe. The optical properties of the materials were investigated upon diffuse reflectance spectra analysis (DRS) using a UV–Vis VARIAN CARY 5 model in the range of 200–600 nm. This instrument was equipped with an integrating sphere of poly-tetrafluoroethylene as reference material. The direct bandgap energy of the synthesised catalysts was estimated using the Tauc plot method [16] using: $(F(R)h\nu)^{1/n} = A(h\nu\text{-}E_g)$. Where *F(R)* is the *Kubelka Munk* function, *h* is the Planck constant, *ν* is the frequency of photon, $n = 1/2$ for direct transitions, *A* is a constant and E_g is the bandgap energy (in eV).

The pH_{pzc} of CoS–$ZnAl_2O_4$ catalyst was estimated as follows: 0.2 g of the catalyst and 0.1 M NaCl were added to different beakers and kept under stirring for 24h (solution pH was adjusted by adding 0.1 M NaOH or HCl), then the final pH (pH_f) was measured. After plotting ΔpH as a function of pH_i, the interaction of the curve with the axis of pH_i determines the pH_{pzc} value.

2.3. Photocatalytic tests

The photocatalytic efficiency of the CoS–$ZnAl_2O_4$ catalyst was evaluated during degradation of Basic blue 41 (BB41) dye ($C_{20}H_{26}N_4O_6S_2$), which shows maximum absorption at λ_{max} = 610 nm [17]. Initial adsorption tests were carried out in the dark to evaluate the absorbance capacity of the catalyst. In this case, a 20-ppm solution of the dye was mixed with a concentration of 1 g/l of the catalyst under stirring conditions (700 rpm) for 30 min until absorption equilibrium. The photocatalytic testing was carried out under these conditions in a 250 ml reactor, with additional air bubbling and light irradiation. The light source was an *Osram Ultra- Vitalux* lamp (300 W) with a polyester UV filter sheet (*Edmund Optics*), showing 99.9% cut-off below 390 nm. The irradiance under these conditions was 140 W/m^2 as measured using a *Photopic PMA21300* sensor with spectral response in the range of 400–700 nm. During the photocatalytic tests, aliquots were collected and centrifuged to remove residual traces of the catalyst. The reaction was monitored using UV–Vis spectroscopy (*J.P. SELECTA, S.A. VR-2000*) at λ_{max} = 610 nm. The degradation of BB41 dye was estimated using: $Degradation\ (\%) = [(C_0\text{–}C)/C_0]\times 100$, where C_0 and C and are the initial concentration and concentration after irradiation time *t*, respectively. The mineralization of the BB41 dye was further monitored using Total Organic Carbon (TOC) analysis in a *Shimadzu TOC-V CPH* analyser: $TOC\ (\%) = [1\text{-}(final\ TOC/initial\ TOC)]\ x100$. To study the stability of the CoS–$ZnAl_2O_4$ catalyst, cycling experiments were carried out under similar conditions. In each cycle, the catalyst was collected by centrifugation, washed with distilled water and dried at 100 °C prior to use in the following cycle.

3. Results and discussion

3.1. Characterisation of the CoS–$ZnAl_2O_4$ catalyst

SEM micrographs of the as-prepared samples are shown in Fig. 1. Pristine $ZnAl_2O_4$ (Fig. 1a-**b**) showed agglomerated particles of a broad range of sizes. This is unsurprising as the sample was dried and crushed prior to analysis. The CoS phase (Fig. 1c–d) showed microflowerlike-like structures, in agreement with previous observations [18]. Both species were identified visually in the CoS–$ZnAl_2O_4$ catalyst (Fig. 1e–f). Rough estimation of crystallite size showed no significant variation between pristine $ZnAl_2O_4$ and the spinel phase in the CoS–$ZnAl_2O_4$ system (Table S1), which suggests there was no structural change after the deposition of the CoS phase. Elemental analysis confirmed the main composition of the samples (Figs. 3S and 4S). Furthermore, particle size

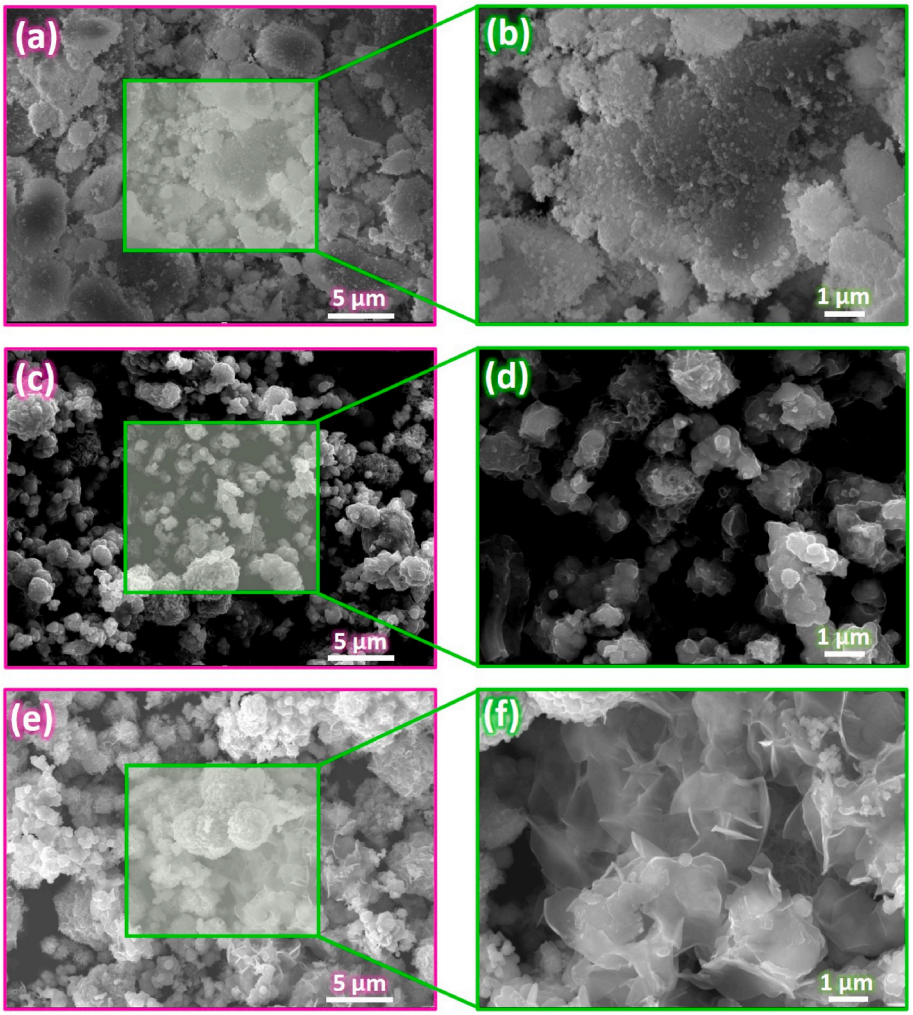

Fig. 1. SEM micrographs of the as-prepared samples: (a,b) Pristine $ZnAl_2O_4$; (c,d) Pristine CoS and (e,f) CoS–$ZnAl_2O_4$ catalyst.

distribution of the CoS–$ZnAl_2O_4$ catalyst was estimated from the SEM images using ImageJ software. The obtained data were analyzed using the Gaussian Distribution fitting. As shown in Fig. S1, the particle size of CoS–$ZnAl_2O_4$ ranges from 1 to 3.5 µm.

The two individual components of the CoS–$ZnAl_2O_4$ catalyst were identified by XRD analysis (Fig. 2). The XRD pattern of the spinel $ZnAl_2O_4$ phase (JCPDS: 05–0669) exhibits the main diffraction peaks at *ca.* 31°, 36°, 44°, 49°, 55°, 59° and 65° (2θ. These features were also clearly observed in the pattern of the CoS–$ZnAl_2O_4$ catalyst. The diffraction peaks of the octahedral CoS phase (JCPDS: 75–0605) were broad and weak, positioned around 30°, 35°, 47° and 54° [19]. Among these, only the peak around 35° could be clearly identified in the CoS–$ZnAl_2O_4$ pattern, together with a shoulder around 54°. The presence of other potential Co_xS_y phases could not be ruled out due to the broadening of the peaks.

Further structural analysis for CoS–$ZnAl_2O_4$ was carried out using X-ray photoelectron spectroscopy (XPS) (Fig. 3). The. The XPS spectra of the Zn peak (Fig. 3a) show the Zn $2p_{3/2}$ and Zn $2p_{1/2}$ at 1022.5 eV and 1045.6 eV, respectively besides, Al 2*p* peak is observed at 75.2 eV (Fig. 3b) [20]. As shown in the Co 2*p* spectrum (Fig. 3c), the deconvoluted peak at 781.7 eV can be attributed to Co $2p_{3/2}$, moreover, the peaks at 794 and 797.9 eV correspond to Co $2p_{1/2}$ [21]. On the other hand, the binding energies of S (2*p*) (Fig. 3d) at 162.7 and 163.3 eV belong to S_2^{2-} of CoS [21,22].

Fig. 4a presents the results of the diffuse reflectance spectra analysis, which was used to evaluate the optical properties of the as-prepared samples. As expected from its wide bandgap, pristine $ZnAl_2O_4$ shows photon absorption in the UV region. On the other hand, CoS shows strong absorption across the UVA and visible light regions, which is consistent with previous reports [23]. The CoS–$ZnAl_2O_4$ catalyst has a wide absorption band combining the optical properties of the two individual components. This combination promotes an efficient harvesting of photons across the entire solar spectrum. A linear fit intersection of the corresponding Tauc plots (Fig. 4b) allowed for the estimation of bandgap energies given as 1.60 eV and 3.95 eV, respectively for CoS and $ZnAl_2O_4$ phases, in agreement with literature values [24]. Two optical transitions were estimated for the CoS–$ZnAl_2O_4$ catalyst, at 1.47 eV and 2.53 eV.

3.2. *Photocatalytic properties of the CoS–$ZnAl_2O_4$ catalyst*

Several photocatalytic tests were carried out following the degradation of 20 ppm of BB41 solution using 1 g/l of each catalyst under visible light irradiation (Fig. 5). An initial adsorption period was allowed for 30 min in the dark until equilibrium. As shown in Fig. 5a, the BB41 dye was stable and did not experience photolysis in the absence of a catalyst under irradiation. Commercial (*P25*) TiO_2 was used as a reference photocatalyst to check the efficiency of the cut-off filter under the illumination conditions of these experiments. The fact that TiO_2 did not show activity under the irradiation conditions used is reassuring since this material is only active in the UV range. This is also the case for $ZnAl_2O_4$, which can only harvest photons in the UV range. In contrast,

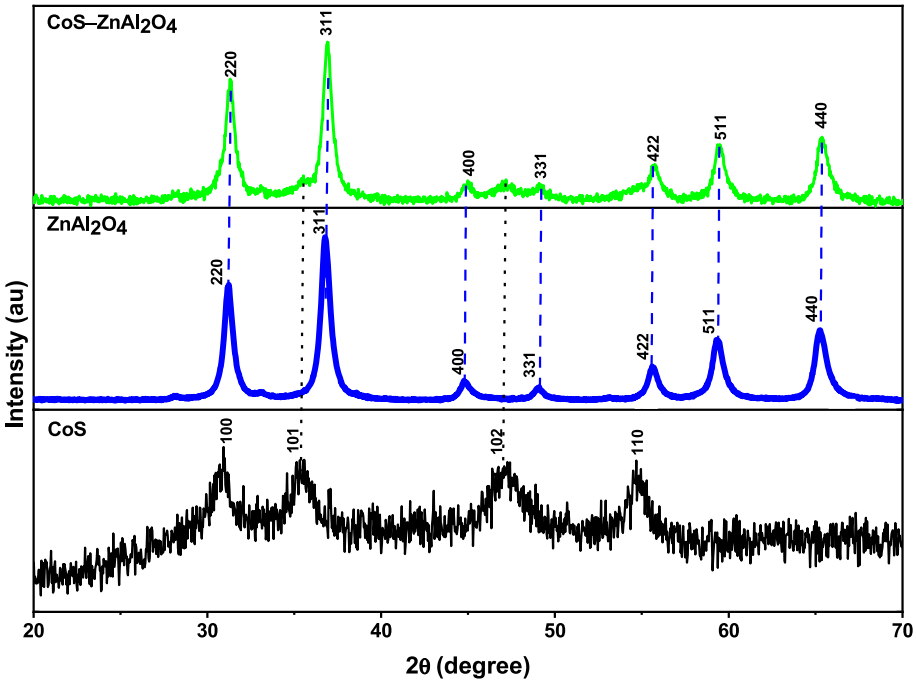

Fig. 2. XRD patterns of the CoS–$ZnAl_2O_4$ catalyst and its individual components.

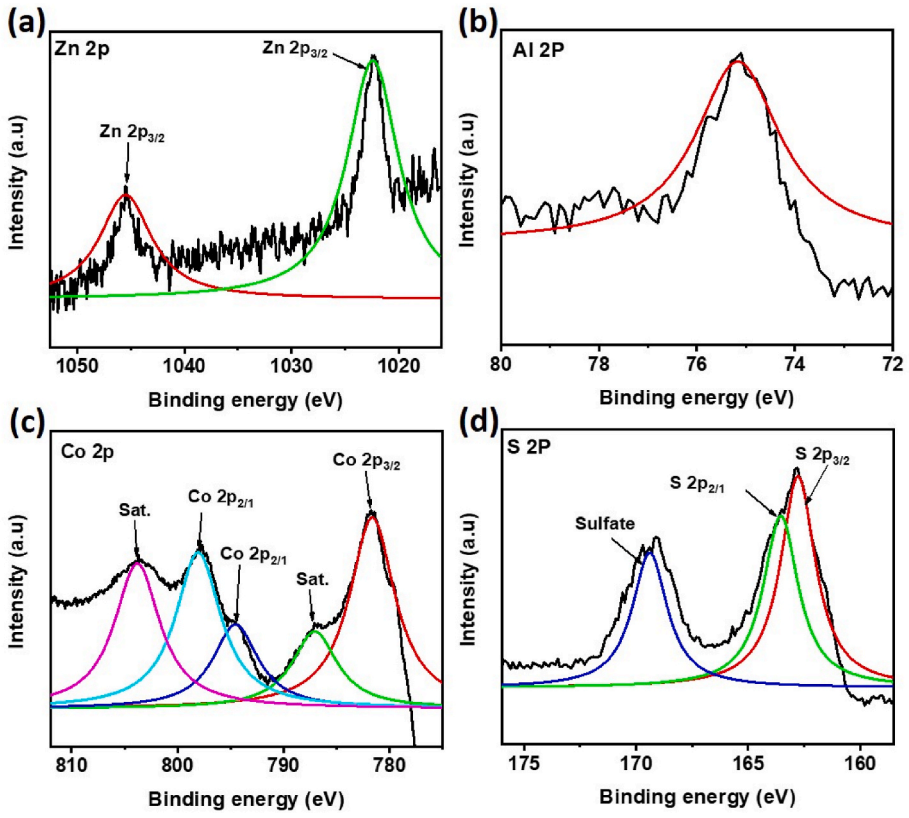

Fig. 3. XPS spectra of (a) Zn 2p, (b) Al 2p, (c) Co 2p and (d) S 2p for the CoS–$ZnAl_2O_4$.

CoS could promote the degradation of the dye up to 40% of the initial concentration within the illumination period of the experiments (t = 80 min). As mentioned above, this material is a narrow bandgap semiconductor and can take advantage of low energy photons to carry out the photodegradation process. The dark adsorption of the CoS–$ZnAl_2O_4$ catalyst was similar to the combined adsorptions of its individual components (Fig. 5a). Upon illumination, however, the full degradation of the dye (100%) took place within the time of the experiments, demonstrating an enhanced efficiency of the photocatalytic system. This was confirmed upon estimation of pseudo first-order kinetics, given as $ln\ (C/C_0) = kt$ (Fig. 5b). The calculated rate constants (k) for each catalyst were 5.0×10^{-3}, 8.6×10^{-3} and 55.6×10^{-3} min^{-1} for $ZnAl_2O_4$, CoS

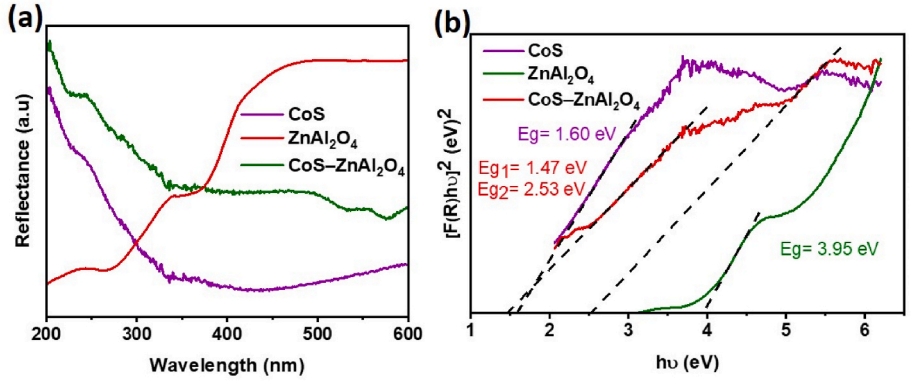

Fig. 4. (a) UV–vis diffuse reflectance spectra and (b) Tauc plots $(F(R)h\upsilon)^2$ vs $(h\upsilon)$) of the CoS, $ZnAl_2O_4$ and CoS–$ZnAl_2O_4$ catalysts.

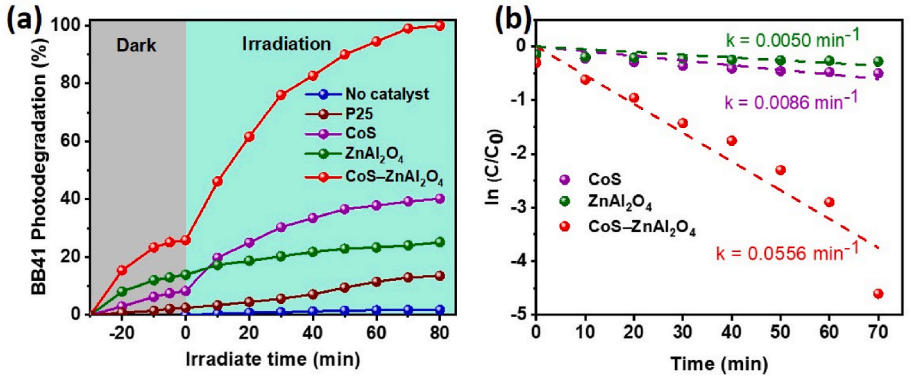

Fig. 5. (a) Photodegradation of BB41 dye on commercial (*P25*) TiO_2, CoS–$ZnAl_2O_4$, $ZnAl_2O_4$ and CoS catalysts under visible light illumination. An adsorption period of the dye in dark was included until equilibrium. The photolysis of the dye in the absence of a catalyst is included as reference. (b) Corresponding photodegradation rates given as ln (C/C_0) versus irradiation time.

and CoS–$ZnAl_2O_4$, respectively. On the other hand, the TOC removal was found 91% while using CoS–$ZnAl_2O_4$ which indicates a good mineralization percentage of BB41 and confirmed the photocatalytic efficiency of the CoS–$ZnAl_2O_4$ catalyst.

The significant enhancement of the photocatalytic rate was attributed to the potential electronic interaction between the two components in the CoS–$ZnAl_2O_4$ catalyst. Charge trapping experiments were thus designed to identify the active species responsible for the degradation of BB41 dye on the catalyst. These tests were carried out using appropriate scavengers under the same experimental conditions as the photodegradation tests. [25] The impact of these scavengers is shown in Fig. 6. As shown, the addition of silver nitrate (SN) (scavenger for e^-) and ethylene diamine tetra-acetic acid (EDTA-2Na) (scavenger for h^+) had no prominent impact (80–90%) in the photodegradation of the dye. In contrast, the addition of isopropanol (IPA) (scavenger for $^{\cdot}OH$) and benzoquinone (BQ) (scavenger for $^{\cdot}O_2^-$) significantly decreased the photodegradation efficiency to 30–40%, which suggests these reactive oxygen species (ROS) were the main drivers of the photocatalytic process.

Taking into account electronegativity values for the two semiconductors −respectively 6.15 eV [26] and 5.49 eV [27] for CoS and $ZnAl_2O_4$, it was possible to estimate the energy of the valence band (E_{VB}) and the conduction band (E_{CB}) edges of each material using the following equations [28]:

$$E_{VB} = \chi - E_0 + 0.5\ E_g$$

$$E_{CB} = E_{VB} - E_g$$

Where E_0 is the free electrons energy on the hydrogen scale; E_g is the bandgap energy; and χ is the semiconductor electronegativity. From these equations, the calculated E_{CB} for CoS and $ZnAl_2O_4$ were 0.85 eV and −0.98 eV, respectively.

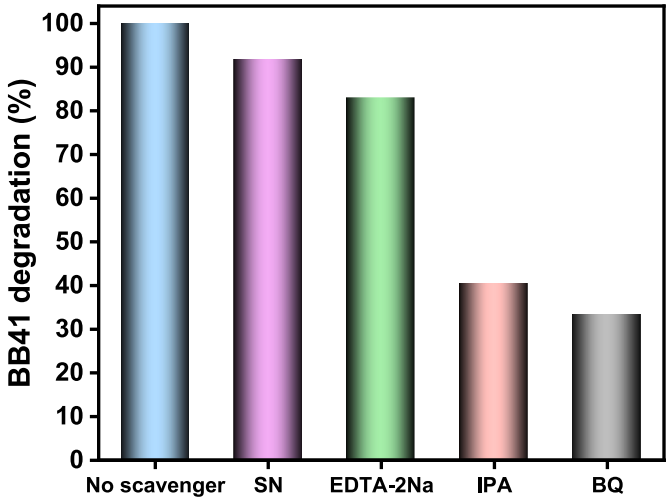

Fig. 6. Trapping experiments of active species using appropriate scavengers [25] during photodegradation of BB41 dye over the CoS–$ZnAl_2O_4$ system. The graph shows relative degradation (%) compared to the reaction in the absence of scavenger (given as 100%). The scavengers used were: silver nitrate (SN) (scavenger for e−); ethylene diamine tetra-acetic acid (EDTA-2Na) (scavenger for h+); isopropanol (IPA) (scavenger of $^{\cdot}OH$); and benzoquinone (BQ) (scavenger of $\cdot O_2^-$).

Based on the results of trapping experiments and the literature, it was

possible to propose a photocatalytic mechanism for the degradation of BB41 by CoS–$ZnAl_2O_4$ catalyst as presented in Fig. 7. CoS and $ZnAl_2O_4$ are both a n-type semiconductor [29,30], for those semiconductors type, the Fermi energy level is close to the E_{CB} [31]. When CoS–$ZnAl_2O_4$ n–n heterojunction photocatalyst was formed, the energy band of CoS and $ZnAl_2O_4$ would move until reach an equilibration state of Fermi level, simultaneously, an inner electric field would be created in the interface of n–n heterojunction [32,33], consequently, the conduction band (CB) and the valence band (VB) of CoS are higher than those of $ZnAl_2O_4$. $ZnAl_2O_4$ is a wide bandgap semiconductor, its large bandgap of 3.95 eV (Fig. 4) can't allow him to be responding under visible light irradiation, on the contrary, the narrow bandgap of CoS (1.60 eV) (Fig. 4) is suitable to be active as photocatalyst under visible light illumination. When the CoS–$ZnAl_2O_4$ catalyst was exposed to the visible irradiation, the electrons e^- will be photogenerated and moved from the VB of CoS to its CB leaving the holes h^+ in the VB, thereafter, the e^- will be transferred to CB of $ZnAl_2O_4$. The CB of $ZnAl_2O_4$ has the higher reduction ability owing to the larger electrical potential difference compared the potential of $O_2/{\cdot}O_2^-$ at −0.33 eV [34]. Thus, the electrons at BC of $ZnAl_2O_4$ could react with O_2 dissolved in water to produce the superoxide radicals (${\cdot}O_2^-$), on the other hand, the potential of VB of CoS is more positive than that of ·OH/OH^- (1.99 eV) [34], which could allow to the holes to react with OH^- to generate hydroxyl radicals ·OH. Finally,${\cdot}O_2^-$ and ·OH will degrade BB41 molecules following equations (1)–(6) as was confirmed by the trapping experiments. Furthermore, the IEF surface was crucial for the enhancement of the photogenerated electrons separation from the CB of CoS to that of $ZnAl_2O_4$ and thus reducing the h^+/e^- recombination, all of this make from CoS–$ZnAl_2O_4$ a system that exhibits enhanced photocatalytic activity for the degradation of BB41 [32].

$$CoS + h\upsilon \rightarrow CoS\ (e^- + h^+) \quad (1)$$

$$CoS\ (e^-) \rightarrow ZnAl_2O_4\ (e^-) \quad (2)$$

$$ZnAl_2O_4\ (e^-) + O_2 \rightarrow {\cdot}O_2^- \quad (3)$$

$$CoS\ (h^+) + OH^- \rightarrow {\cdot}OH \quad (4)$$

$${\cdot}O_2^- + BB41 \rightarrow Degradation \quad (5)$$

$${\cdot}OH + BB41 \rightarrow Degradation \quad (6)$$

3.3. Effect of operational parameters and catalyst stability

Further photocatalytic testing included evaluation of operational parameters, namely catalyst amount concentration of the dye and pH (Fig. 8a–c). The full degradation of the dye (100%, 20 ppm) was reached using catalyst concentrations of 1 g/L and 1.5 g/L in solutions at its natural initial pH (7.5) and at room temperature, while a loading of 0.5 g/L achieved a degradation rate of 71% (Fig. 8a). Maximum degradation can thus be established within the range of 0.5–1 g/L of catalyst loading at a dye concentration of 20 ppm. The catalyst efficiency (at 1 g/L) remains the same over 20–30 ppm dye concentration, decreasing slightly upon further dye loadings (Fig. 8b). This is probably due to a screening effect, with high concentration of the dye hindering photon absorption at the catalyst surface, as it has been suggested in similar studies [35].

The effect of pH was significant in the photodegradation mechanism of the dye, as expected. BB41 is a cationic dye and an alkaline environment would promote dye adsorption on the catalyst surface [36]. The photodegradation process was evaluated under different pH (1 g/l, 20 ppm) using appropriate aliquots of HCl/NaOH 0.1 M solutions (Fig. 8c). A full degradation rate remained stable up to pH 7, dropping to nearly 50% at pH 3. Beyond hindering dye adsorption, this observation can be related to a decrease in hydroxyl radical concentration, following the reaction mechanism described above. In addition, the acidic environment could promote particle agglomeration, with an impact on effective surface area and photon absorption [37]. Moreover, the found pH_{PZC} value is 7.2 (Fig. S6), above this value, the catalyst surface is negatively charged while below it the surface becomes positively charged, which will promote attraction between catalyst surface and BB41 dye and thus enhancing more its photodegradation.

Further studies evaluated the stability of the CoS–$ZnAl_2O_4$ catalyst under the experimental conditions used in this work (Fig. 8d). The material was used over 5 cycles following the procedure described in the experimental section. The efficiency observed remained close to 90% based on the bleaching of the dye, with less than 10% change in TOC removal over the cycling tests. Table 1 shows comparison of the photocatalytic efficiency of a range of materials during BB41 removal. The data collected here suggest that the CoS–$ZnAl_2O_4$ catalyst can be a competitive material for the treatment of textile wastewater under solar conditions.

4. Conclusions

A CoS-supported $ZnAl_2O_4$ catalyst was successfully prepared by a hydrothermal method for photodegradation of basic blue 41 (BB41) dye under visible light illumination. UV–vis diffusive reflectance spectroscopy demonstrated that the CoS–$ZnAl_2O_4$ catalyst showed an extended absorption band along the UV and visible light regions. The combined properties of CoS and $ZnAl_2O_4$ promoted the efficient photodegradation of the dye upon absorption of low energy photons, which demonstrates its potential for solar applications. Further studies presented in this work included operational parameters and stability tests to evaluate the practical use of the photocatalyst. Comparison with other proposed systems demonstrates the competitive ability of our material for the treatment of textile wastewater, which is one of the main sources of water pollution worldwide. Similar systems combining sulphides and spinel structures may be studied towards further optimisation, following the basis of the current work.

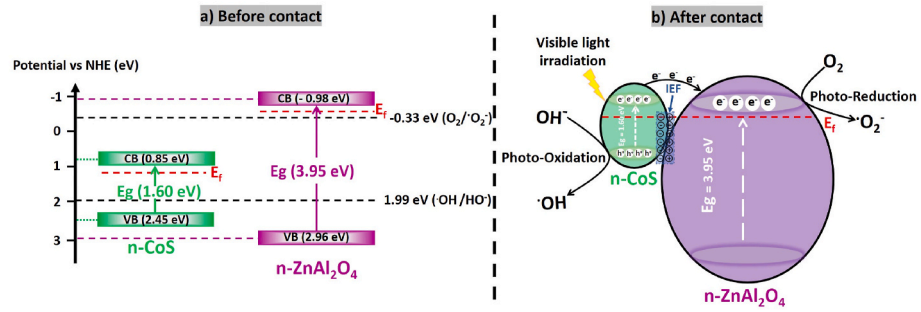

Fig. 7. Proposed mechanism of photodegradation of BB41 by CoS–$ZnAl_2O_4$catalyst under visible light illumination.

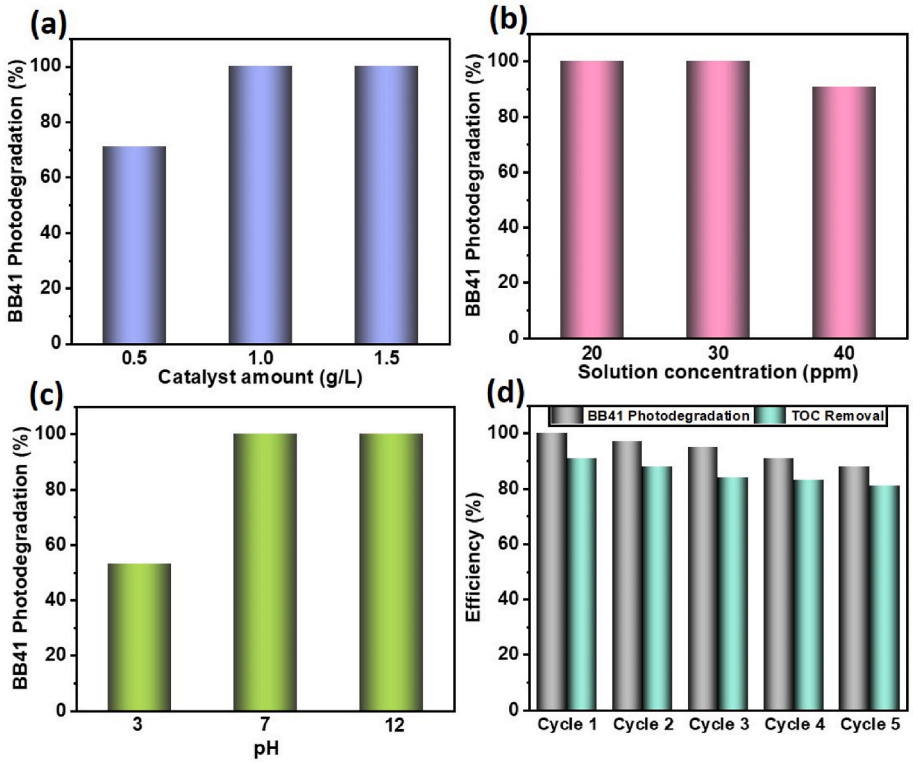

Fig. 8. (a) Influence of catalyst concentration in the photodegradation of BB41 dye (20 ppm). (b) Influence of dye concentration at constant catalyst loading (1 g/L). (c) Influence of pH using a dye concentration of 20 ppm and catalyst loading of 1 g/L. (d) Cycle experiments (20 ppm, 1 g/L) showing BB41 photodegradation rates (%) and total organic carbon (TOC) measurements.

Table 1
Comparison among previous reports and the CoS–$ZnAl_2O_4$ catalyst during BB41 removal under a range of experimental conditions.

Photocatalyst	Dye concentration (ppm)	Catalyst amount (g/l)	Degradation efficiency (%)	Degradation time (min)	Light source	Reference
CoS–$ZnAl_2O_4$	20	1	100	80	Visible light	Present work
$SrTiO_3/Ag_3PO_4$	20	0.5	99	80	Visible light	[38]
$CoCr_2O_4$	10	0.5	99	300	Visible light	[39]
$Bi_{12}NiO_{19}$	15	1	98	180	Visible light	[40]
C/ZnO/Zn	12.5	0.1	96	45	UV light	[41]
MOF-199	15	0.04	99	180	UV light	[42]
ZnO	20	0.02	72.56	180	UV light	[43]
TiO_2–ZnO	20	10	≈100	60	Sunlight	[36]

Funding

This paper received no funding or grant.

CRediT authorship contribution statement

Youssef Fahoul: Conceptualization, Methodology, Investigation, Data curation, Formal analysis, Writing – review & editing. **Karim Tanji:** Investigation, Data curation, Writing – original draft, Writing – review & editing. **Oscar Manuel González Díaz:** Conceptualization, Methodology, Writing – review & editing. **Raúl Quesada-Cabrera:** Conceptualization, Methodology, Writing – review & editing. **Yassine Naciri:** Investigation, Data curation, Writing – original draft, Writing – review & editing. **Imane El Mrabet:** Investigation, Data curation, Writing – original draft, Writing – review & editing. **Abdelali El Gaidoumi:** Formal analysis, Writing – review & editing. **José Miguel Doña Rodríguez:** Supervision, Writing – review & editing. **Abdelhak Kherbeche:** Supervision, Writing – review & editing.

Declaration of competing interest

The authors declare that they have no known competing financial interests or personal relationships that could have appeared to influence the work reported in this paper.

Data availability

No data was used for the research described in the article.

Acknowledgement

We thank Dr. Sanjayan Sathasivam for XPS analysis and discussion. OMGD would like to thank the Spanish Ministry of Science and Innovation for funding (Project PID2020-118720RB-I00, PHOTOREDOX). RQC would like to thank the Ministry of Education and Vocational Training (Beatriz Galindo Program) and the Agency for Research, Innovation and the Information Society (ACIISI) in the Canary Islands (Project PROID2021010047, DESALASOLAR). JMDR and OMGD would also like to thank the Spanish Ministry of Science and Innovation and ERDF funds for infrastructure (UNLP10-3E-726).

Appendix A. Supplementary data

Supplementary data to this article can be found online at https://doi.org/10.1016/j.optmat.2023.114148.

References

[1] Destination Zero: Seven Years of Detoxing the Clothing Industry, (n.d.).
[2] P.A. Pekakis, N.P. Xekoukoulotakis, D. Mantzavinos, Treatment of textile dyehouse wastewater by TiO2 photocatalysis, Water Res. 40 (2006) 1276–1286, https://doi.org/10.1016/J.WATRES.2006.01.019.
[3] S. Chakrabarti, B.K. Dutta, Photocatalytic degradation of model textile dyes in wastewater using ZnO as semiconductor catalyst, J. Hazard Mater. 112 (2004) 269–278, https://doi.org/10.1016/J.JHAZMAT.2004.05.013.
[4] C. Liu, D. Yang, Y. Jiao, Y. Tian, Y. Wang, Z. Jiang, Biomimetic synthesis of TiO2–SiO2–Ag nanocomposites with enhanced visible-light photocatalytic activity, ACS Appl. Mater. Interfaces 5 (2013) 3824–3832, https://doi.org/10.1021/AM4004733.
[5] S. Balachandran, M. Swaminathan, Facile fabrication of heterostructured Bi2O3–ZnO photocatalyst and its enhanced photocatalytic activity, J. Phys. Chem. C 116 (2012) 26306–26312, https://doi.org/10.1021/JP306874Z.
[6] M. Fu, Y. Li, S. Wu, P. Lu, J. Liu, F. Dong, Sol–gel preparation and enhanced photocatalytic performance of Cu-doped ZnO nanoparticles, Appl. Surf. Sci. 258 (2011) 1587–1591, https://doi.org/10.1016/J.APSUSC.2011.10.003.
[7] T. Ali, A. Ahmed, U. Alam, I. Uddin, P. Tripathi, M. Muneer, Enhanced photocatalytic and antibacterial activities of Ag-doped TiO2 nanoparticles under visible light, Mater. Chem. Phys. 212 (2018) 325–335, https://doi.org/10.1016/J.MATCHEMPHYS.2018.03.052.
[8] M. Saeed, M. Muneer, A. ul Haq, N. Akram, Photocatalysis: an effective tool for photodegradation of dyes—a review, 2021 29:1, Environ. Sci. Pollut. Res. 29 (2021) 293–311, https://doi.org/10.1007/S11356-021-16389-7.
[9] P. Shah, A. Unnarkat, F. Patel, M. Shah, P. Shah, A comprehensive review on spinel based novel catalysts for visible light assisted dye degradation, Process Saf. Environ. Protect. 161 (2022) 703–722, https://doi.org/10.1016/j.psep.2022.03.030.
[10] N. Shaheen, M.A. Yousuf, I. Shakir, S. Zulfiqar, P.O. Agboola, M.F. Warsi, Wet chemical route synthesis of spinel oxide nano-catalysts for photocatalytic applications, Phys. B Condens. Matter 580 (2020), 411820, https://doi.org/10.1016/j.physb.2019.411820.
[11] S. Battiston, C. Rigo, E. Da Cruz Severo, M.A. Mazutti, R.C. Kuhn, A. Gündel, E. L. Foletto, Synthesis of zinc aluminate (ZnAl2O4) Spinel and its application as photocatalyst, Mater. Res. 17 (2014) 734–738, https://doi.org/10.1590/S1516-14392014005000073.
[12] Q. Tian, M. Ran, G. Fang, L. Ding, A. Pan, K. Shen, Y. Deng, ZnAl2O4/BiPO4 composites as a heterogeneous catalyst for photo-Fenton treatment of textile and pulping wastewater, Sep. Purif. Technol. 239 (2020), 116574, https://doi.org/10.1016/J.SEPPUR.2020.116574.
[13] P. Shah, A. Unnarkat, F. Patel, M. Shah, P. Shah, A comprehensive review on spinel based novel catalysts for visible light assisted dye degradation, Process Saf. Environ. Protect. 161 (2022) 703–722, https://doi.org/10.1016/j.psep.2022.03.030.
[14] T. Tatarchuk, B. Al-Najar, M. Bououdina, M.A. Aal Ahmed, Catalytic and photocatalytic properties of oxide spinel, s (2019), https://doi.org/10.1007/978-3-319-68255-6_158.
[15] L. Zou, H. Wang, G. Yuan, X. Wang, Magnetically separable CdS/ZnFe2O4 composites with highly efficient photocatalytic activity and photostability under visible light, ACS Appl. Nano Mater. 1 (2018) 831–838, https://doi.org/10.1021/ACSANM.7B00243.
[16] A. Pandey, G. Jain, D. Vyas, S. Irusta, S. Sharma, Nonreducible, basic La2O3 to reducible, acidic La2-xSbxO3 with significant oxygen storage capacity, lower band gap, and effect on the catalytic activity, J. Phys. Chem. C 121 (2017) 481–489, https://doi.org/10.1021/ACS.JPCC.6B10821.
[17] M. Gougazeh, F. Kooli, J.C. Buhl, Removal efficiency of basic blue 41 by three zeolites prepared from natural Jordanian kaolin, Clays Clay Miner 67 (2019) 143–153, https://doi.org/10.1007/S42860-019-00016-1.
[18] J. Li, Y. Liu, X. Tang, L. Xu, L. Min, Y. Xue, X. Hu, Z. Yang, Multiwalled carbon nanotubes coated with cobalt(II) sulfide nanoparticles for electrochemical sensing of glucose via direct electron transfer to glucose oxidase, Microchim. Acta 187 (2020) 1–9, https://doi.org/10.1007/S00604-019-4047-8.
[19] H. Zhong, J. Xi, P. Tang, D. Li, Y. Feng, Positive effect of heat treatment on carbon-supported CoS nanocatalysts for oxygen reduction reaction, 2015, Catalysts 5 (5) (2015) 1211–1220, https://doi.org/10.3390/CATAL5031211, 1211–1220.
[20] A.Q. Wang, J.X. Wang, H. Wang, Y.N. Huang, M.L. Xu, X.L. Wu, Synthesis of SO 4 2−/TiO 2 –ZnAl 2 O 4 composite solid acids as the esterification catalysts, RSC Adv. 7 (2017) 14224–14232, https://doi.org/10.1039/C7RA01386H.
[21] Z. Wang, W. Zeng, K.Y.S. Ng, Facile synthesis of CoS nanoparticles anchored on the surface of functionalized multiwalled carbon nanotubes as cathode materials for advanced Li-S batteries, Ind. Eng. Chem. Res. 61 (2022) 9322–9330, https://doi.org/10.1021/ACS.IECR.2C01222.
[22] H. Liu, G. Cui, L. Li, Z. Zhang, X. Lv, X. Wang, Polypyrrole chains decorated on CoS spheres: a core-shell like heterostructure for high-performance microwave absorption, 2020, Nanomaterials 10 (2020) 166, https://doi.org/10.3390/NANO10010166, 166. 10.
[23] B. Yu, F. Meng, T. Zhou, A. Fan, Z. Zhao, M.W. Khan, Construction of CoS/CeO2 heterostructure nanocages with enhanced photocatalytic performance under visible light, J. Am. Ceram. Soc. 103 (2020) 6136–6148, https://doi.org/10.1111/JACE.17340.
[24] G. Govindasamy, P. Murugasen, S. Sagadevan, Optical and electrical properties of chemical bath deposited cobalt sulphide thin films, Mater. Res. 20 (2016) 62–67, https://doi.org/10.1590/1980-5373-MR-2016-0441.
[25] Y. Naciri, A. Hsini, Z. Ajmal, A. Bouddouch, B. Bakiz, J.A. Navío, A. Albourine, J. C. Valmalette, M. Ezahri, A. Benlhachemi, Influence of Sr-doping on structural, optical and photocatalytic properties of synthesized Ca3(PO4)2, J. Colloid Interface Sci. 572 (2020) 269–280, https://doi.org/10.1016/J.JCIS.2020.03.105.
[26] Z. Liu, J. Xu, Q. Liang, Y. Li, H. Yu, CoS/ZnWO4 composite with band gap matching: simple impregnation synthesis, efficient dye sensitization system for hydrogen production, J. Nanoparticle Res. 22 (2020) 1–11, https://doi.org/10.1007/S11051-020-04857-Z.
[27] Q. Tian, M. Ran, G. Fang, L. Ding, A. Pan, K. Shen, Y. Deng, ZnAl2O4/BiPO4 composites as a heterogeneous catalyst for photo-Fenton treatment of textile and pulping wastewater, Sep. Purif. Technol. 239 (2020), 116574, https://doi.org/10.1016/J.SEPPUR.2020.116574.
[28] Q. Tian, M. Ran, G. Fang, L. Ding, A. Pan, K. Shen, Y. Deng, ZnAl2O4/BiPO4 composites as a heterogeneous catalyst for photo-Fenton treatment of textile and pulping wastewater, Sep. Purif. Technol. 239 (2020), https://doi.org/10.1016/j.seppur.2020.116574.
[29] M. Jain, Manju, R. Kumar, S.O. Won, K.H. Chae, A. Vij, A. Thakur, Defect states and kinetic parameter analysis of ZnAl2O4 nanocrystals by X-ray photoelectron spectroscopy and thermoluminescence, 2020 10:1. Scientific Reports 10 (2020) 1–14, https://doi.org/10.1038/s41598-019-57227-8.
[30] Z. Jin, X. Wang, In situ XPS proved efficient charge transfer and ion adsorption of ZnCo2O4/CoS S-Scheme heterojunctions for photocatalytic hydrogen evolution, Mater. Today Energy 30 (2022), 101164, https://doi.org/10.1016/J.MTENER.2022.101164.
[31] H. jian Zhao, R.J. Wu, X.C. Wang, Y. min An, W.X. Zhao, F. Ma, Heterojunction of BiPO4/BiOBr photocatalysts for Rhodamine B dye degradation under visible LED light irradiation, J. Chin. Chem. Soc. 67 (2020) 1016–1023, https://doi.org/10.1002/JCCS.201900344.
[32] X. Zhou, Y. Chen, P. Wang, C. Xu, Q. Yan, Fabrication of AgI/BiPO4 n–n heterojunction photocatalyst for efficient degradation of organic pollutants, J. Mater. Sci. Mater. Electron. 31 (2020) 12638–12648, https://doi.org/10.1007/S10854-020-03814-9.
[33] K. Wang, Z. Qian, W. Guo, Multi-heterojunction of SnO2/Bi2O3/BiOI nanofibers: facile fabrication with enhanced visible-light photocatalytic performance, Mater. Res. Bull. 111 (2019) 202–211, https://doi.org/10.1016/J.MATERRESBULL.2018.11.005.
[34] Y. Gong, Y. Wu, Y. Xu, L. Li, C. Li, X. Liu, L. Niu, All-solid-state Z-scheme CdTe/TiO2 heterostructure photocatalysts with enhanced visible-light photocatalytic degradation of antibiotic waste water, Chem. Eng. J. 350 (2018) 257–267, https://doi.org/10.1016/J.CEJ.2018.05.186.
[35] K. Tanji, J.A. Navio, J. Naja, M.C. Hidalgo, A. Chaqroune, C. Jaramillo-Páez, A. Kherbeche, Extraordinary visible photocatalytic activity of a Co0.2Zn0.8O system studied in the Remazol BB oxidation, J. Photochem. Photobiol. Chem. 382 (2019), 111877, https://doi.org/10.1016/J.JPHOTOCHEM.2019.111877.
[36] Y. Jiang, Y. Sun, H. Liu, F. Zhu, H. Yin, Solar photocatalytic decolorization of C.I. Basic Blue 41 in an aqueous suspension of TiO2–ZnO, Dyes Pigments 78 (2008) 77–83, https://doi.org/10.1016/J.DYEPIG.2007.10.009.
[37] M. Shanthi, V. Kuzhalosai, Photocatalytic degradation of an azo dye, Acid Red 27, 03, in: Aqueous Solution Using Nano ZnO 51A, IJC-A, 2012 [March 2012].
[38] S. Kafian, A. Sadeghzadeh-Attar, Photocatalytic degradation of Basic Blue 41 dye under visible light over SrTiO3/Ag3PO4 hetero-nanostructures, Int. J. Appl. Ceram. Technol. 19 (2022) 3347–3357, https://doi.org/10.1111/IJAC.14148.
[39] Y. Benrighi, N. Nasrallah, T. Chaabane, V. Sivasankar, A. Darchen, O. Baaloudj, Characterization of CoCr2O4 semiconductor: a prominent photocatalyst in the degradation of basic blue 41 from wastewater, Opt. Mater. 122 (2021), 111819, https://doi.org/10.1016/J.OPTMAT.2021.111819.
[40] B. Brahimi, H. Kenfoud, Y. Benrighi, O. Baaloudj, Structural and optical properties of Bi12NiO19 sillenite crystals: application for the removal of basic blue 41 from wastewater, 2021, Photochem 1 (1) (2021) 319–329, https://doi.org/10.3390/PHOTOCHEM1030020, 319–329.
[41] S. Lanfredi, M.A.L. Nobre, P.S. Poon, J. Matos, Hybrid material based on an amorphous-carbon matrix and ZnO/Zn for the solar photocatalytic degradation of basic blue 41, 2020, Molecules 25 (96. 25) (2019) 96, https://doi.org/10.3390/MOLECULES25010096.
[42] N.M. Mahmoodi, J. Abdi, Nanoporous metal-organic framework (MOF-199): synthesis, characterization and photocatalytic degradation of Basic Blue 41, Microchem. J. 144 (2019) 436–442, https://doi.org/10.1016/J.MICROC.2018.09.033.
[43] N.M. Mahmoodi, S. Keshavarzi, M. Ghezelbash, Synthesis of nanoparticle and modelling of its photocatalytic dye degradation ability from colored wastewater, J. Environ. Chem. Eng. 5 (2017) 3684–3689, https://doi.org/10.1016/J.JECE.2017.07.010.